Image resolution and image contrast in the electron microscope. II. Elastic scattering and incoherent illumination

1973 J. Phys. A: Math. Nucl. Gen. 6 205

(http://iopscience.iop.org/0301-0015/6/2/011)

J. Phys. A: Math., Nucl. Gen., Vol. 6, February 1973. Printed in Great Britain.

Image resolution and image contrast in the electron microscope II. Elastic scattering and incoherent illumination

D L Misell

Department of Physics, Queen Elizabeth College, Campden Hill Road, London W8 7AH, UK

MS received 26 July 1972

Abstract. The present work evaluates the effect of lens aberrations on image resolution and image contrast in the transmission electron microscope for the elastic component of the electron beam. The effect of spatially and chromatically incoherent illumination on image resolution and image contrast is examined. For spatially incoherent illumination the relationship between the object structure and the image intensity is an improvement on that obtained with coherent illumination; this improvement in image resolution is offset by a loss in image contrast as a result of using spatially incoherent illumination. The adverse effect of chromatic incoherence on image resolution is evaluated. The effect of chromatic aberration on image resolution is significant at 20 keV but only becomes important at 100 keV if the energy spread of the incident electron beam exceeds 2 eV. The loss in image contrast as a result of chromatic incoherence is about 50% for 20 keV electrons and less than 20% for 100 keV electrons.

1. Introduction

In this paper we examine the effects of electron source incoherence on image resolution and image contrast in the transmission electron microscope. It is well known that the use of an incoherent source gives an image which may bear a closer relationship to the object structure (eg Lenz 1965, Barakat 1970) than in the case of coherent illumination. We consider first spatial incoherence where the angular distribution $F(\boldsymbol{K}_0)$ characterizes the angular variation of the incident electron wavevector $\boldsymbol{K}_0$. The image intensity $j_i(\boldsymbol{r}_i)$ is calculated from the incoherent superposition of elastically scattered electron waves with different $\boldsymbol{K}_0$, that is (Lenz 1971, Misell 1971),

$$j_i(\boldsymbol{r}_i) = \int \left| \int \psi_0(\boldsymbol{r}_0) G(\boldsymbol{r}_i - \boldsymbol{r}_0) \exp(i\boldsymbol{K}_0 \cdot \boldsymbol{r}_0)\, d\boldsymbol{r}_0 \right|^2 F(\boldsymbol{K}_0)\, d\boldsymbol{K}_0 \tag{1}$$

where $\psi_0(\boldsymbol{r}_0)$ is the electron wavefunction immediately after transmission through the specimen and $G(\boldsymbol{r})$ is the resolution function of the objective lens, including spherical aberration and defocusing (see Misell 1973, to be referred to as I). In the case of complete spatial incoherence ($F(\boldsymbol{K}_0)$ = constant) equation (1) becomes (eg Lenz 1965)

$$j_i(\boldsymbol{r}_i) = \int |\psi_0(\boldsymbol{r}_0)|^2 |G(\boldsymbol{r}_i - \boldsymbol{r}_0)|^2\, d\boldsymbol{r}_0 \tag{2}$$

which is an intensity convolution integral.

In § 2 we examine for spatial incoherence the effect of the diffraction limit on the image intensity (§ 2.1), the condition for maximum image contrast at a point corresponding to the centre of an object (§ 2.2) and, under the defocus conditions for maximum contrast, the relationship between the object structure and image intensity (§ 2.3). The intermediate case of partial source coherence, which is more complex than either complete coherence or complete incoherence, has been considered by Hanszen and Trepte (1971b), although image resolution was not examined in their work.

Secondly we consider chromatic incoherence arising from the energy distribution $N(E)$ of the incident electron beam. The image intensity is then calculated by the incoherent superposition of electrons with different E (Misell 1971)

$$j_i(\boldsymbol{r}_i) = \int_{-\infty}^{+\infty} \left| \int \psi_0(\boldsymbol{r}_0) G(E, \boldsymbol{r}_i - \boldsymbol{r}_0)\, \mathrm{d}\boldsymbol{r}_0 \right|^2 N(E)\, \mathrm{d}E \tag{3}$$

where $G(E, \boldsymbol{r}_i - \boldsymbol{r}_0)$ is the resolution function including a chromatic aberration term. The Fourier transform of $G(E, \boldsymbol{r})$, $T(E, \mathbf{v})$, is given by (Kanaya 1956, Hanszen and Trepte 1971a, Misell 1971)

with
$$\left.\begin{aligned} T(E, \mathbf{v}) &= \exp\left(-\frac{2\pi \mathrm{i}}{\lambda(E)} W(E, \mathbf{v})\right) B(\mathbf{v}) \\ W(E, \mathbf{v}) &= \frac{C_s \lambda(E)^4}{4} v^4 + \frac{C_c E \lambda(E)^2}{2E_0} v^2 + \frac{\Delta f}{2} \lambda(E)^2 v^2 \end{aligned}\right\} \tag{4}$$

C_c is the third order chromatic aberration constant and the electron wavelength $\lambda(E)$ is formally dependent on the variation E from the incident electron energy E_0. In § 3 we examine the effect of chromatic incoherence on image resolution and image contrast, firstly in the absence of spherical aberration (§ 3.1), and secondly including spherical aberration (§ 3.2) in addition to chromatic aberration.

2. The effect of spatial incoherence on the image

From equation (2) it is seen that the phase information on $\psi_0(\boldsymbol{r}_0)$ is irretrievably lost using spatially incoherent illumination. Thus equation (2) may be inverted to give information only on $|\psi_0(\boldsymbol{r}_0)|$. If we consider a weak phase–weak amplitude object

$$\psi_0(\boldsymbol{r}_0) \simeq 1 + \mathrm{i}\eta(\boldsymbol{r}_0) - \epsilon(\boldsymbol{r}_0) \tag{5}$$

$|\psi_0(\boldsymbol{r}_0)|^2 = 1 - 2\epsilon(\boldsymbol{r}_0) + \epsilon(\boldsymbol{r}_0)^2 + \eta(\boldsymbol{r}_0)^2$ and since both η and ϵ are much less than unity $|\psi_0(\boldsymbol{r}_0)|^2 \simeq 1 - 2\epsilon(\boldsymbol{r}_0)$, that is, we obtain mainly amplitude information on the object structure. In the present work we have calculated the image intensity for a gaussian structure, that is $A \exp(-br_0^2)$ for both η and ϵ, with $A \simeq 0{\cdot}1$, $b = 20\ \mathrm{nm}^{-1}$ (see I). As is conventional for a convolution function, $|G(\boldsymbol{r})|^2$ is normalized, that is,

$$\int |G(\boldsymbol{r})|^2\, \mathrm{d}\boldsymbol{r} = 1$$

or from Parseval's theorem

$$\int |G(\boldsymbol{r})|^2\, \mathrm{d}\boldsymbol{r} = \int |T(\mathbf{v})|^2\, \mathrm{d}\mathbf{v} = \int B(\mathbf{v})^2\, \mathrm{d}\mathbf{v} \tag{6}$$

and the last integral has a value of $\pi v_{\max}^2$ for a circular aperture of semi-angle $\alpha = \lambda_0 v_{\max}$.

Hence

$$|G(\mathbf{r})|^2 = \frac{1}{4\pi v_{\max}^2}(q(\mathbf{r})^2 + q_1(\mathbf{r})^2) \tag{7}$$

with $q(\mathbf{r}) = F^{-1}\{2\sin(K_0 W(\mathbf{v}))B(\mathbf{v})\}$ and $q_1(\mathbf{r}) = F^{-1}\{2\cos(K_0 W(\mathbf{v}))B(\mathbf{v})\}$ (see I). It is noted that, unlike the case with spatially coherent illumination, there is no distinction between bright field ($B(0) = 1$) and dark field microscopy ($B(0) = 0$) because of the large angle of illumination of the specimen; in the coherent case the directional property of the incident electron beam is represented by a delta function.

2.1. The effect of the diffraction limit on the image

First we consider the effect of the finite objective aperture size on image resolution and image contrast, in the absence of spherical aberration ($C_s = 0$); this represents the extent to which we can reproduce the original object structure with finite objective aperture. The resolution function $|G(\mathbf{r})|^2$ is then

$$\left(\frac{J_1(2\pi v_{\max} r)}{2\pi v_{\max} r}\right)^2 4\pi v_{\max}^2;$$

$|G(\mathbf{r})|^2$ is shown in figure 1 for $E_0 = 20$ keV for $\alpha = 0{\cdot}01, 0{\cdot}015, 0{\cdot}02$ rad (figure 1(*a*)) and $E_0 = 100$ keV for $\alpha = 0{\cdot}005, 0{\cdot}01, 0{\cdot}015$ rad (figure 1(*b*)). We note that the radial half-width $r_{1/2}$ of $|G(\mathbf{r})|^2$ is significantly less than the corresponding coherent resolution function, for example, $E_0 = 100$ keV, $\alpha = 0{\cdot}01$, $r_{1/2} = 0{\cdot}19$ nm for $|G(\mathbf{r})|^2$ and $r_{1/2} = 0{\cdot}26$ nm for $G(\mathbf{r})$. The radial convergence of $|G(\mathbf{r})|^2$ is also preferable to the oscillatory behaviour of $G(\mathbf{r})$; however, image resolution is not always as important as the image contrast, which is reduced by a factor of about four using incoherent illumination (see § 2.2). Figures 1(*c* and *d*) show the results for the convolution of $|G(\mathbf{r})|^2$ with $|\psi_0(\mathbf{r}_0)|^2$, corresponding to the resolution functions of figures 1(*a* and *b*) respectively; the background level of unity has been subtracted from the results and the dotted curve represents the gaussian structure. The gaussian structure ($r_{1/2} = 0{\cdot}37$ nm) is quite well produced for the larger objective aperture: $E_0 = 20$ keV, $\alpha = 0{\cdot}02$ rad, $r_{1/2} = 0{\cdot}44$ nm; $E_0 = 100$ keV, $\alpha = 0{\cdot}01$ rad, $r_{1/2} = 0{\cdot}42$ nm, $\alpha = 0{\cdot}015$ rad, $r_{1/2} = 0{\cdot}40$ nm.

2.2. The condition for maximum image contrast

Corresponding to $\mathbf{r}_i = 0$, we calculate the image contrast $C_i(0)$ variation with the defocus value of the objective lens for spatially incoherent illumination; $C_s = 2$ mm in all calculations. The results for $C_i(0)$ with 20 keV and 100 keV electrons are shown respectively in figures 2(*a* and *b*). We note that the largest image contrast value occurs for $\alpha = 0{\cdot}01$ rad, $E_0 = 20$ keV but from figure 1(*c*) this aperture will produce diffraction limited results. It is preferable to use larger objective aperture sizes and to correct for the increased lens aberrations, avoiding the difficult problem of eliminating the diffraction limit by analytic contination. The intrinsic image resolution obtained using the larger aperture, $\alpha = 0{\cdot}02$ ($E_0 = 20$ keV), is better than that obtained with the smaller apertures. However, if image contrast is of prime importance α should be about 0·01 rad for both 20 keV and 100 keV. Table 1 gives the values for Δf_{opt} corresponding to the maximum value of $C_i(0)$ (column 3); only the main maximum is considered. In the calculations presented below we shall examine the image intensity distributions for $\Delta f_{\text{opt}} \pm 50$ nm for $\alpha = 0{\cdot}02$ ($E_0 = 20$ keV), $\alpha = 0{\cdot}01, 0{\cdot}015$ rad ($E_0 = 100$ keV).

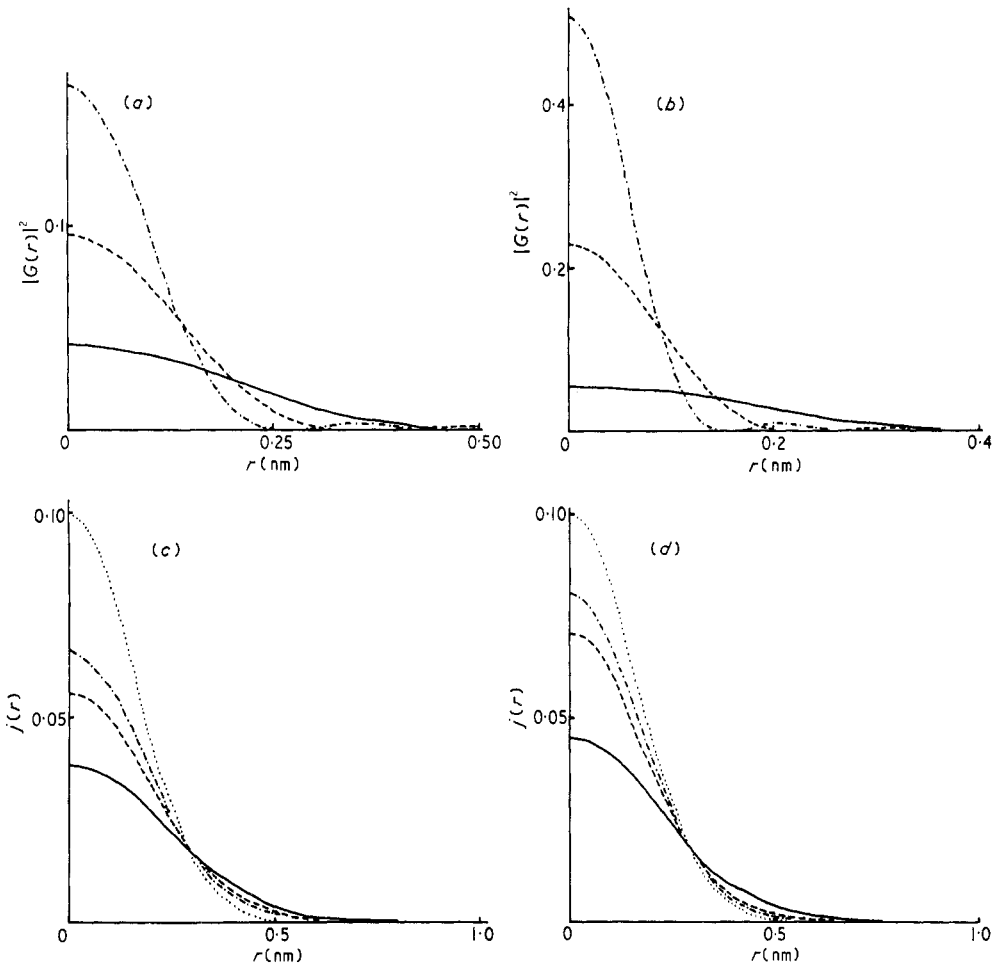

Figure 1. The effect of the diffraction limit on the image intensity for spatially incoherent illumination. The resolution function $|G(r)|^2$ is shown for: (*a*) $E_0 = 20$ keV; full curve, $\alpha = 0{\cdot}01$ rad; broken curve, $\alpha = 0{\cdot}015$ rad; chain curve, $\alpha = 0{\cdot}02$ rad; (*b*) $E_0 = 100$ keV; full curve, $\alpha = 0{\cdot}005$ rad; broken curve, $\alpha = 0{\cdot}01$ rad; chain curve, $\alpha = 0{\cdot}015$ rad. (*c*) and (*d*) are the corresponding image intensity distributions $j(r)$. The dotted curve represents the gaussian structure.

It is noted that the image contrast for spatially incoherent illumination varies between 0·02 and 0·04, a factor of four below the maxima (or minima) in $C_i(0)$ for coherent illumination (0·08 to 0·16).

We find, as in the case of coherent illumination, that the behaviour of the resolution function at $r = 0$, $|G(0)|^2$ reproduces the condition for maximum contrast and is thus a model independent determination of Δf_{opt} (see table 1, column 4).

2.3. The image intensity distributions

In figures 3(*a*, *b*, *c*) we present results for the resolution function $|G(r)|^2$ calculated for $(\Delta f_{opt} - 50)$nm (full curves), Δf_{opt} (broken curves) and $(\Delta f_{opt} + 50)$nm (chain curves),

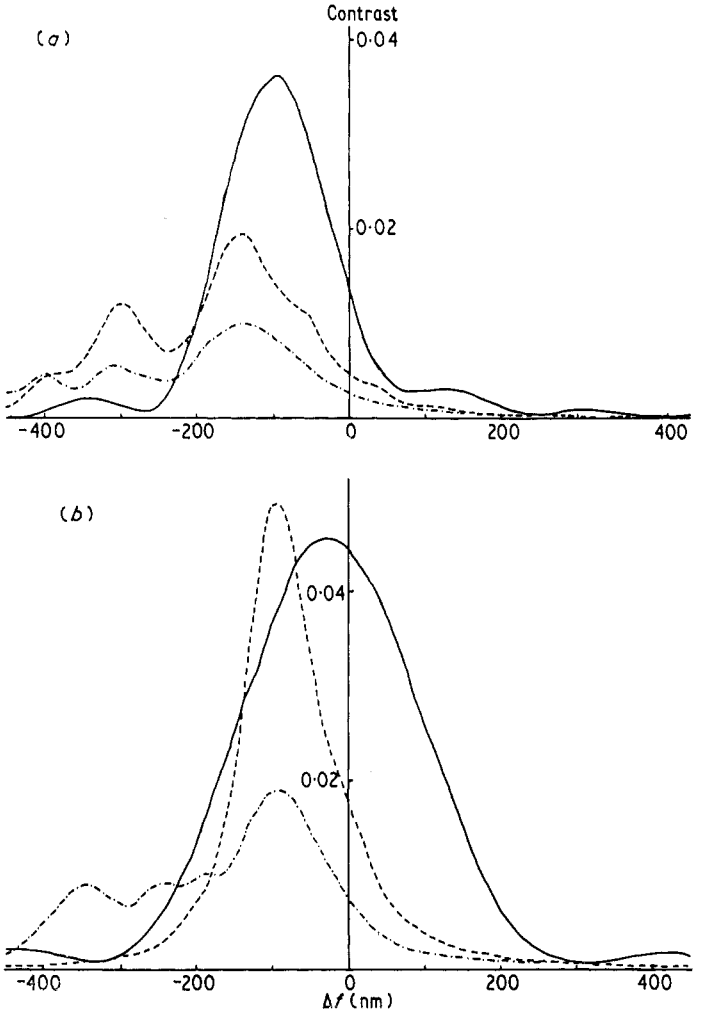

Figure 2. The image contrast $C_i(0)$ as a function of defocus, Δf nm, for spatially incoherent illumination. (*a*) $E_0 = 20$ keV; full curve, $\alpha = 0{\cdot}01$ rad; broken curve, $\alpha = 0{\cdot}015$ rad; chain curve, $\alpha = 0{\cdot}02$ rad. (*b*) $E_0 = 100$ keV; full curve, $\alpha = 0{\cdot}005$ rad; broken curve, $\alpha = 0{\cdot}01$ rad; chain curve, $\alpha = 0{\cdot}015$ rad. $C_s = 2$ mm.

Table 1. The optimum defocus value Δf_{opt} nm for maximum image contrast using spatially incoherent illumination and its dependence on the incident electron energy E_0 keV and objective aperture semi-angle α rad. $C_s = 2$ mm.

E_0(keV)	α(rad)	Δf_{opt} (nm) (model)	Δf_{opt} (nm) (resolution function)
20	0·01	−100	−100
20	0·015	−140	−150
20	0·02	−140	−140
100	0·005	−20	−20
100	0·01	−100	−100
100	0·015	−90	−90

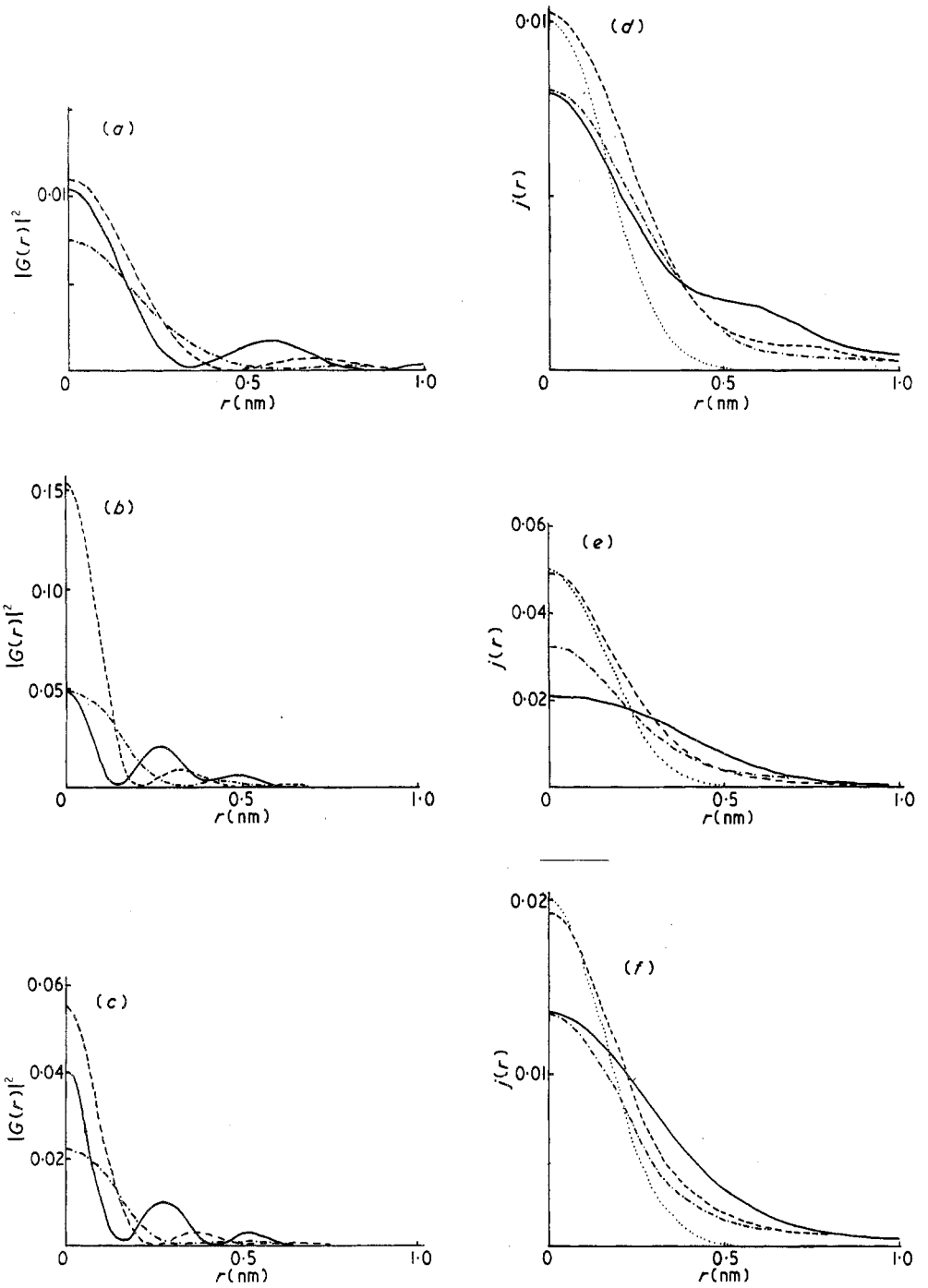

Figure 3. The image intensity distributions for spatially incoherent illumination. The resolution function $|G(r)|^2$ is shown for: (*a*) $\alpha = 0{\cdot}02$ rad, $E_0 = 20$ keV; (*b*) $\alpha = 0{\cdot}01$ rad, $E_0 = 100$ keV; (*c*) $\alpha = 0{\cdot}015$ rad, $E_0 = 100$ keV for $(\Delta f_{opt} - 50)$ nm (full curves), Δf_{opt} (broken curves), $(\Delta f_{opt} + 50)$ nm (chain curves). (*d*), (*e*) and (*f*) show the corresponding intensity distributions $j(r)$ with the gaussian structure shown by a dotted curve. $C_s = 2$ mm.

where ± 50 nm is considered as the precision of defocus. It is seen that the radial convergence of $|G(r)|^2$ is excellent for Δf_{opt}, although the radial halfwidth of this $|G(r)|^2$ is not necessarily the smallest. We note that resolution functions corresponding to subsidiary maxima on the $C_i(0)$ curve, for example, $\Delta f \simeq -200$ to -350 nm for $\alpha = 0{\cdot}015$, $E_0 = 100$ keV, do not give such good radial convergence. The corresponding image intensity distributions are shown in figures 3(*d*, *e*, *f*) in comparison with the gaussian structure (dotted curves scaled to fit on the appropriate $j(r)$ axis); the background intensity has been subtracted from these curves. The most notable point is the close similarity between the gaussian structure and $j_i(r_i)$, and the absence of large subsidiary maxima in $j_i(r_i)$ such as occurred in the corresponding coherent images (see I). The close similarity between the object structure and image intensity is offset by the very low image contrast, which is below 5% for $A = 0{\cdot}1$ in the gaussian model. There is clearly no point in obtaining improved resolution if the image contrast is too low. This point is emphasized by electron micrographs taken of biological specimens, where certain structural features cannot be distinguished from the background (+ noise) using incoherent illumination (Hibi and Takahashi 1971).

3. The effect of chromatic incoherence on the image

In this section we examine the effect of the energy distribution of the incident electron beam on image resolution in the absence of spherical aberration (§ 3.1) and on image resolution including both spherical and chromatic aberration (§ 3.2); in the conventional transmission electron microscope the thermal spread of the incident electron beam is less than 2 eV and in the scanning transmission microscope, with a field emission source, $N(E)$ has a halfwidth of about 0·2 eV. We show below that the chromatic incoherence of the source is important only at low incident electron energies ($E_0 \simeq 20$ keV).

Equation (3) for the image intensity $j_i(r_i)$ may be rewritten for a weak phase–weak amplitude object (equation (5)) as a convolution integral (in bright field microscopy)

$$j_i(r_i) = 1 + \int \eta(r_0) u(r_i - r_0)\, dr_0 - \int \epsilon(r_0) u_1(r_i - r_0)\, dr_0 \tag{8}$$

where the resolution functions $u(r)$ and $u_1(r)$ are given by (Misell 1971)

$$u(r) = \int \{\mathrm{Re}(L(\mathbf{v}))Q(\mathbf{v}) + \mathrm{Im}(L(\mathbf{v}))Q_1(\mathbf{v})\}\, d\mathbf{v} \tag{9}$$

and

$$u_1(r) = \int \{\mathrm{Re}(L(\mathbf{v}))Q_1(\mathbf{v}) + \mathrm{Im}(L(\mathbf{v}))Q(\mathbf{v})\}\, d\mathbf{v}. \tag{10}$$

Re and Im denote the real and imaginary parts of $L(\mathbf{v})$, which is derived from the Fourier transform of $N(E)$ (Hanszen and Trepte 1971a, Misell 1971):

$$L(\mathbf{v}) = \int_{-\infty}^{+\infty} N(E) \exp\left(-\frac{iK_0 C_c \lambda_0^2 E v^2}{2E_0}\right) dE \tag{11}$$

with the approximation $\lambda(E) = \lambda_0$.

In the present calculations, we took as an approximation to $N(E)$ a gaussian distribution and then $\mathrm{Im}(L(\mathbf{v})) = 0$. The chromatic aberration constant $C_c = 2$ mm in all calculations.

3.1. The effect of chromatic aberration on the image

In order to investigate the effect of only chromatic aberration on the image resolution we consider $C_s = 0, \Delta f = 0$ and examine the dependence of chromatic aberration on the objective aperture size for $N(E)$ of varying energy halfwidths $E_{1/2}$. This study is complicated by the resolution limit due to diffraction at the objective aperture and for comparison we present the corresponding results for $E_{1/2} = 0$.

In figure 4 we present the resolution function $G_1(r) = F^{-1}(B(\mathbf{v})L(\mathbf{v}))$ for $E_0 = 20$ keV and three α values: 0·01 rad (figure 4(*a*)), 0·015 rad (figure 4(*b*)) and 0·02 rad (figure 4(*c*)). As expected because of the $\theta^2(v^2)$ dependence of the chromatic aberration term in

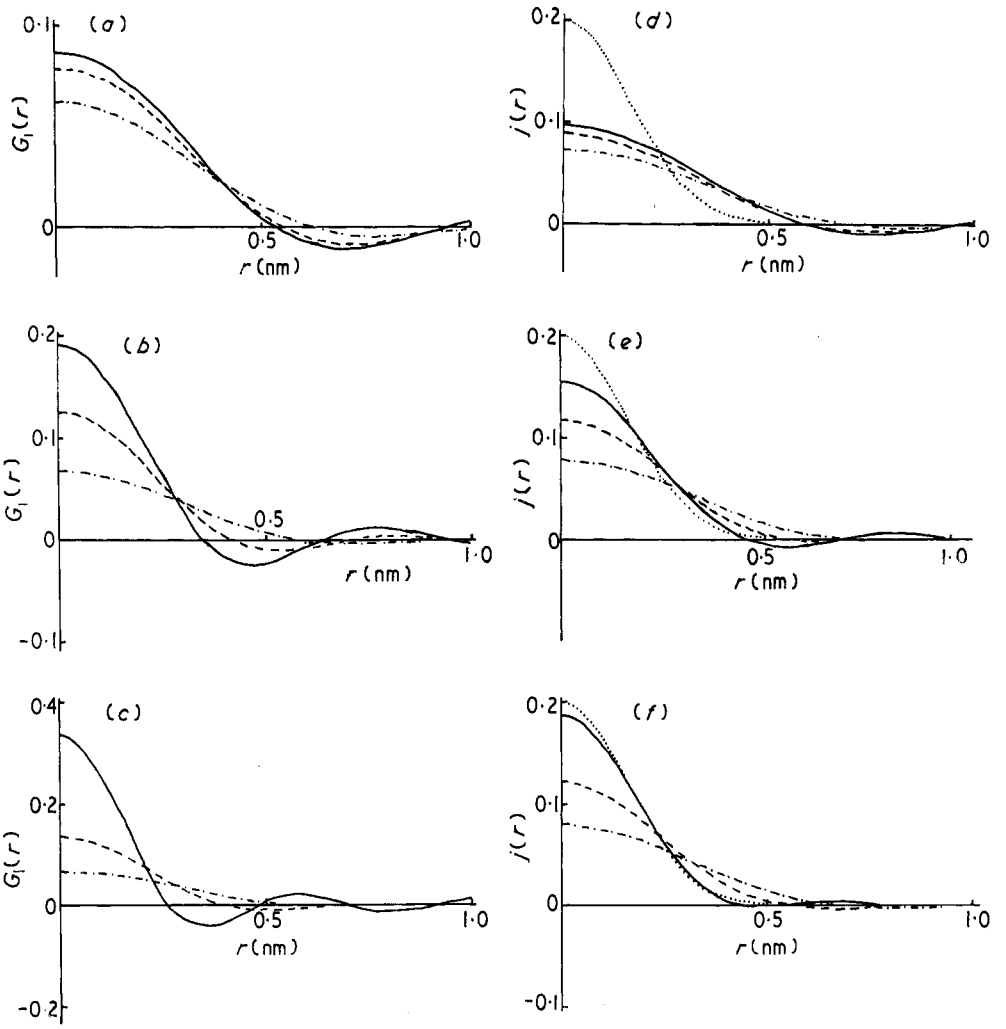

Figure 4. The image intensity distributions for chromatically incoherent illumination, $E_0 = 20$ keV in the absence of spherical aberration. The resolution function $G_1(r)$ ($C_s = 0$) is shown for: (*a*) $\alpha = 0{\cdot}01$ rad, (*b*) $\alpha = 0{\cdot}015$ rad, (*c*) $\alpha = 0{\cdot}02$ rad; the curves correspond to $E_{1/2} = 0$ eV (full curve), $E_{1/2} = 0{\cdot}5$ eV (broken curve) and $E_{1/2} = 1{\cdot}0$ eV (chain curve). The corresponding image intensity distributions $j(r)$ are shown in (*d*), (*e*) and (*f*) where the dotted curve represents the gaussian structure. $C_c = 2$ mm.

equation (4), the resolution (compared with $E_{1/2} = 0$) deteriorates with increasing α. An estimate of the effect of chromatic aberration is given in table 2 from the radial halfwidth $r_{1/2}$ of the resolution function, where the figures should be taken relative to $r_{1/2}$ for $E_{1/2} = 0$. Comparing at 20 keV $\alpha = 0{\cdot}015$ rad and $\alpha = 0{\cdot}02$ rad we see that,

Table 2. The effect of chromatic aberration on image resolution for chromatically incoherent illumination defined by an energy halfwidth $E_{1/2}$ eV. The radial halfwidth $r_{1/2}$ nm of the resolution function is presented for an objective aperture semi-angle α rad and incident electron energy E_0. $C_c = 2$ mm.

E_0(keV)	α(rad)	$r_{1/2}$(nm) for $E_{1/2}$ =	0 eV	0·5 eV	1 eV	2 eV	10 eV
20	0·01		0·60	0·62	0·67		
20	0·015		0·40	0·46	0·61		
20	0·02		0·30	0·45	0·61		
100	0·005		0·52			0·52	0·60
100	0·01		0·26			0·34	0·56
100	0·015		0·18			0·26	0·56

although $r_{1/2} = 0{\cdot}4$ nm ($\alpha = 0{\cdot}015$ rad) and $r_{1/2} = 0{\cdot}3$ nm ($\alpha = 0{\cdot}02$ rad) for $E_{1/2} = 0$, the radial halfwidths are the same for $E_{1/2} = 1$ eV. Corresponding to the $E_{1/2}$ in the scanning transmission microscope, the loss in resolution due to chromatic aberration at $E_0 = 20$ keV is represented only by a small change in $r_{1/2}$ from 0·3 nm to 0·35 nm for $\alpha = 0{\cdot}02$ rad. The results for $G_1(\boldsymbol{r})$ at 100 keV are shown in figure 5, where the effect of chromatic aberration on image resolution is significant only for $E_{1/2} > 2$ eV. The effect of chromatic aberration is expected to be less than at 20 keV since the chromatic aberration term depends on $E/(\lambda_0 E_0)$, and to obtain results corresponding to $E_{1/2} = 1$ eV at 20 keV, $E_{1/2}$ has to be increased to 10 eV for 100 keV. The results for $E_0 = 100$ keV are in agreement with those of Hanszen and Trepte (1971a), who note that the loss in resolution due to chromatic incoherence is negligible, although the image contrast is affected. Figures 4(*d*, *e*, *f*) and 5(*d*, *e*, *f*) show the corresponding images for the resolution functions given and the gaussian profile is shown by a dotted curve. For $E_0 = 20$ keV (figure 4) the loss in image contrast for $E_{1/2} = 1$ eV is about 50% whereas for $E_0 = 100$ keV (figure 5) the loss in contrast is 10%. (In figure 5(*d*) the full and broken curves coincide for $E_{1/2} = 0$ and $E_{1/2} = 2$ eV with $\alpha = 0{\cdot}005$ rad, and in figure 5(*f*) the dotted and full curves coincide for the gaussian structure and $E_{1/2} = 0$ with $\alpha = 0{\cdot}015$ rad.)

3.2. The combined effect of chromatic and spherical aberration on the image

As may be seen from equation (4) the defocus term $\Delta f\theta^2/2$ has a similar angular dependence to the chromatic aberration term $C_c E\theta^2/2E_0$, and it is expected that the underfocus condition which effectively compensates for spherical aberration will have a similar effect on chromatic aberration (eg Kanaya 1956, Misell 1971). Thus when we consider the effect of both spherical and chromatic aberration on the image resolution, we do not expect the resolution to deteriorate markedly from that obtained in the absence of chromatic aberration, although Δf_{opt} is generally larger (negative) in the former case. We confirm this statement by presenting the results for the resolution function $u(\boldsymbol{r})$ (broken curves in figures 6(*a*, *b*, *c*)) with $q(\boldsymbol{r})$ for chromatically coherent illumination (full curves in figures 6(*a*, *b*, *c*)) corresponding to Δf_{opt} for coherent illumination. It is

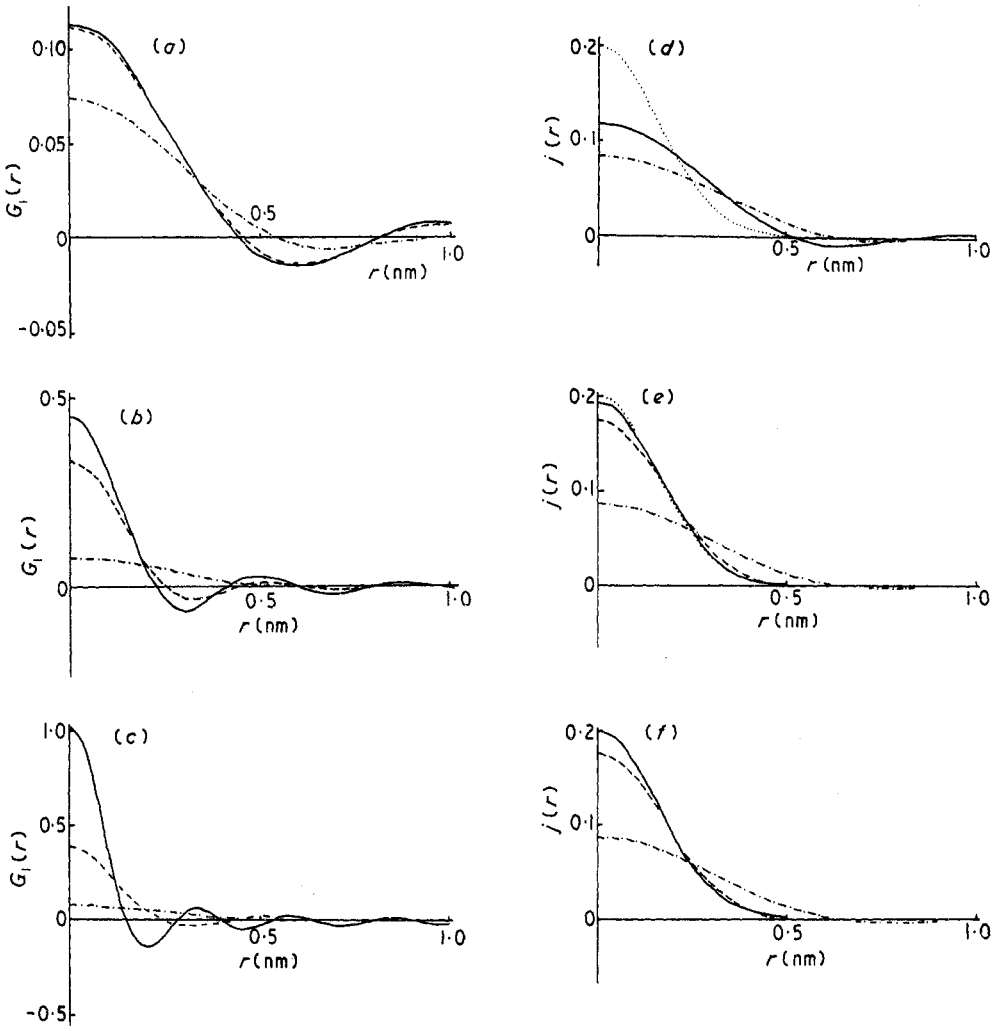

Figure 5. The image intensity distributions for chromatically incoherent illumination, $E_0 = 100$ keV, $C_s = 0$. The resolution function $G_1(r)$ is shown for: (*a*) $\alpha = 0{\cdot}005$ rad, (*b*) $\alpha = 0{\cdot}01$ rad, (*c*) $\alpha = 0{\cdot}015$ rad; the curves correspond to $E_{1/2} = 0$ eV (full curve), $E_{1/2} = 2$ eV (broken curve) and $E_{1/2} = 10$ eV (chain curve). The corresponding image intensity distributions $j(r)$ are shown in (*d*), (*e*) and (*f*) where the dotted curve represents the gaussian structure. $C_c = 2$ mm.

difficult to estimate which resolution function, $u(r)$ or $q(r)$, leads to the best resolution in the image, although the radial halfwidth of $u(r)$ is greater than that of $q(r)$ for these particular defocus values. In fact the main effect of chromatic incoherence is a loss in image contrast rather than any significant deterioration in image resolution. Figures 6(*d*, *e*, *f*) show the phase contrast images (in bright field for a phase object) corresponding to the resolution functions of figures 6(*a*, *b*, *c*). The loss in image contrast due to chromatic incoherence is about 50% for $E_0 = 20$ keV, $\alpha = 0{\cdot}02$ rad, $E_{1/2} = 1$ eV (figures 6(*a*, *d*)) and less than 20% for $E_0 = 100$ keV, $\alpha = 0{\cdot}01/0{\cdot}015$ rad, $E_{1/2} = 2$ eV (figures 6(*b*, *e*) and 6(*c*, *f*)). However, there are certain defocus values where the resolution

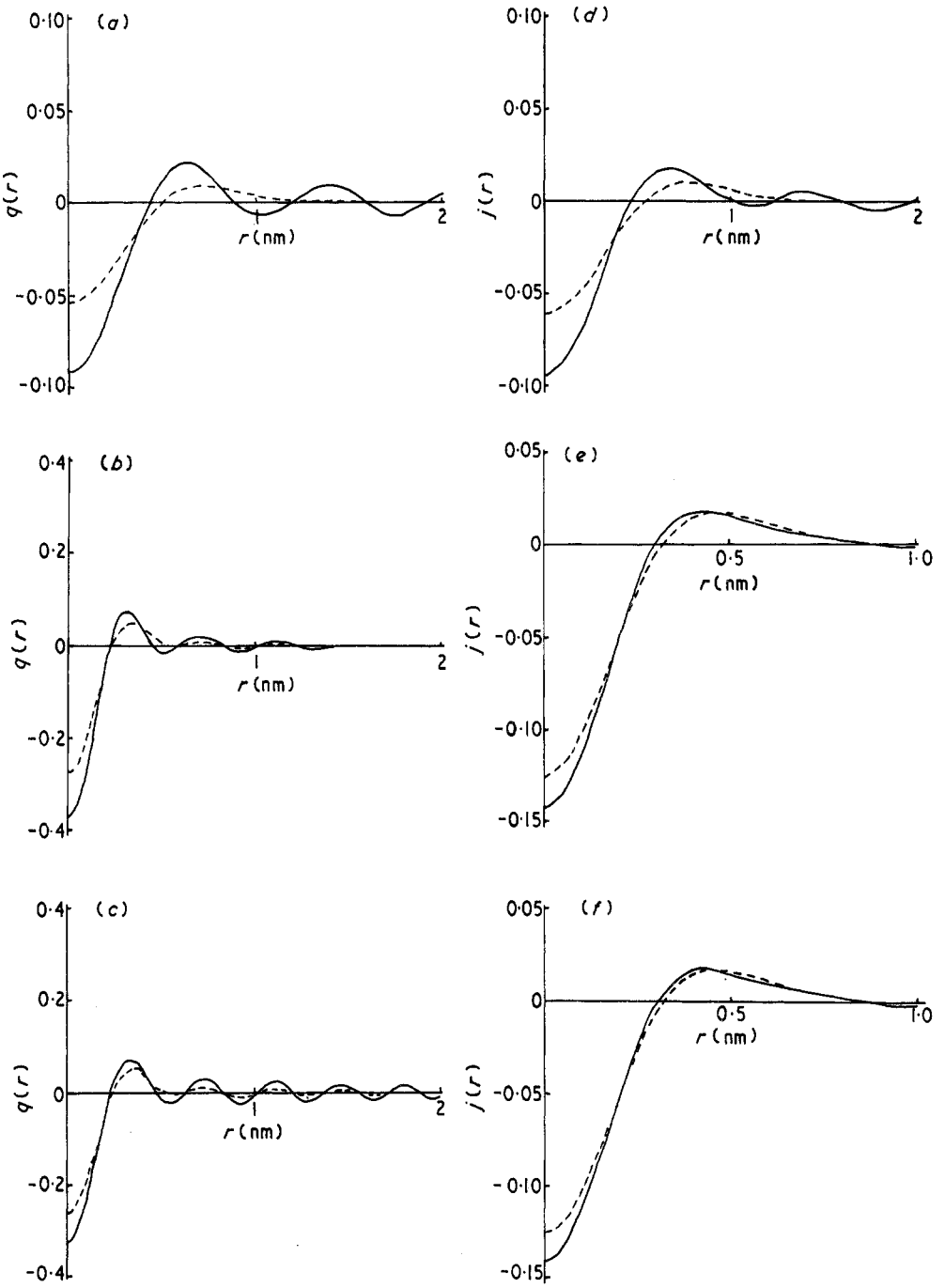

Figure 6. A comparison of the image intensity distributions for coherent illumination (full curve) and chromatically incoherent illumination (broken curve). The resolution function $q(r)$ is shown for: (*a*) $\alpha = 0{\cdot}02$ rad, $E_0 = 20$ keV, $E_{1/2} = 1$ eV; (*b*) $\alpha = 0{\cdot}01$ rad, $E_0 = 100$ keV, $E_{1/2} = 2$ eV; (*c*) $\alpha = 0{\cdot}015$ rad, $E_0 = 100$ keV, $E_{1/2} = 2$ eV. The corresponding image intensity distributions are shown in (*d*), (*e*) and (*f*). In (*a*) $\Delta f = -150$ nm, (*b*) $\Delta f = -100$ nm, (*c*) $\Delta f = -100$ nm. $C_s = 2$ mm, $C_c = 2$ mm.

function $u(r)$ has a smaller radial halfwidth than $q(r)$, although in general the image contrast is inferior to that obtained with coherent illumination.

It is noted that since equation (8) is a convolution integral relating the elastic image intensity in bright field $j_i(r_i)$ to $\eta(r_0)$ and $\epsilon(r_0)$, we may not only correct η and ϵ for spherical aberration and defocusing, but also the chromatic aberration defect. Provided that the energy distribution $N(E)$ has a small energy halfwidth (1–2 eV), the phase structure η can be obtained, unlike the case of spatial incoherence where the phase structure terms are small in comparison with those resulting from ϵ.

4. Conclusions

In the present work we have examined the effect of spatial and chromatic incoherence of the incident electron beam on the bright field elastic image. In particular, it has been shown that spatially incoherent illumination gives a much closer relationship between the object structure and the image intensity than is the case for coherent illumination. However, with this source incoherence we are not able to reconstruct phase structure information (eg $\eta(r_0)$), although the convolution integral relating image intensity $j_i(r_i)$ to $|\psi_0(r_0)|^2$ may be inverted without approximation. Thus with spatially incoherent illumination we obtain information on the amplitude attenuation of the incident electron beam by the specimen, and phase contrast effects are minimal. The case made for low-voltage electron microscopy (E_0 = 5–20 keV) relates to the absence of phase contrast effects in the low voltage microscope and the accentuation of absorption and scattering contrast effects. However, at normal incident electron energies the information carried by the absorption term $\epsilon(r_0)$ may not be as relevant as that obtained from the phase term $\eta(r_0)$, which is sensitive to the structural differences in the specimen. In addition we note that for spatially incoherent illumination the image contrast is reduced by a factor of about four from the contrast obtained with coherent illumination.

The radial dependence of the resolution function $|G(r)|^2$ may be used to determine the optimum defocus Δf_{opt} for maximum image contrast and the best resolution in the image for spatially incoherent illumination.

In the case of chromatically incoherent illumination, the loss in image resolution due to chromatic aberration is estimated to be 0·2–0·5 nm for E_0 = 20 keV for an energy distribution of halfwidth $E_{1/2} \simeq 1$ eV (α = 0·01–0·02 rad) and 0·2 nm for E_0 = 100 keV for $E_{1/2} \simeq 2$ eV (α = 0·01–0·015 rad). However, the loss in image resolution due to chromatic incoherence is secondary to the loss in image contrast. As in the case of spatial incoherence, the appropriate resolution function, $u(r)$ or $u_1(r)$, may be used to determine the optimum defocus value for maximum image contrast and the last image resolution. For chromatic incoherence the phase information ($\eta(r_0)$) is not irretrievably lost and the electron micrograph may be corrected for chromatic aberration in addition to spherical aberration and defocusing, to give a diffraction limited η and ϵ (see I).

The analysis given in the paper applies not only to the conventional microscope but also to the scanning transmission microscope, where the condenser lens system is the equivalent of both the condenser and objective lens of the conventional microscope. Thus the illumination angle α_c is identical to the objective aperture semi-angle α (Zeitler and Thomson 1970). The chromatic incoherence of the electron source in the scanning transmission microscope is small for the normal energy distribution halfwidth of about 0·2 eV, except for large aperture sizes (semi-angle, $\alpha \simeq 0{\cdot}03$ rad subtended at the specimen).

Acknowledgment

The author is grateful to the University of London for the provision of excellent computing facilities.

References

Barakat R 1970 *Optica Acta* **17** 337–47
Hanszen K-J and Trepte L 1971a *Optik* **32** 519–38
—— 1971b *Optik* **33** 166–98
Hibi T and Takahashi S 1971 *J. Electron Microsc., Japan* **20** 17–22
Kanaya K 1956 *Bull. electrotech. Lab., Japan* **20** 801–15
Lenz F 1965 *Optik* **22** 270–88
—— 1971 *Electron Microscopy in Material Science* ed U Valdré (New York: Academic Press) pp 540–69
Misell D L 1971 *J. Phys.* A: *Gen. Phys.* **4** 782–97
—— 1973 *J. Phys.* A: *Math., Nucl. Gen.* **6** 62–78
Zeitler E and Thomson M G R 1970 *Optik* **31** 359–66